Paramagnetic magnetostriction in the chiral magnet CrNb3S6 at room temperature

doi: https://doi.org/10.1103/PhysRevB.105.104412

Paramagnetic magnetostriction in a chiral magnet $CrNb_3S_6$ at room-temperature

Masaki Mito[1,2],* Takayuki Tajiri[3], Yusuke Kousaka[2,4], Yoshihiko Togawa[2,4], Jun Akimitsu[5], Jun-ichiro Kishine[2,6], and Katsuya Inoue[2,7,8]

[1] *Faculty of Engineering, Kyushu Institute of Technology, Kitakyushu 804-8550, Japan*
[2] *Chirality Research Center, Hiroshima University, Higashihiroshima 739-8526, Japan*
[3] *Faculty of Science, Fukuoka University, Fukuoka 814-0180, Japan*
[4] *Graduate School of Engineering, Osaka Prefecture University, Sakai 599-8570, Japan*
[5] *Research Institute for Interdisciplinary Science, Okayama University, Okayama 700-8530, Japan*
[6] *Graduate School of Arts and Sciences, The Open University of Japan, Chiba 261-8586, Japan*
[7] *Graduate School of Science, Hiroshima University, Higashihiroshima 739-8526, Japan and*
[8] *Institute for Advanced Materials Research, Hiroshima University, Higashihiroshima 739-8526, Japan*

(Dated: January 25, 2022)

We report that the magnetostriction (MS) effects occur in a paramagnetic state of a chiral magnet $CrNb_3S_6$. Through a series of experimental tests at room temperature, structural changes were observed at the level of a unit cell. The structural parameters are dependent of the strength and direction of magnetic field (H) even at temperature excessively higher than the magnetic ordering temperature T_c of 127 K. The present paramagnetic MS prominently appeared under $H//$ the ab-plane (easy plane) as opposed to under $H//$ the c-axis. Features observed in the paramagnetic MS effect significantly differ from those of the spontaneous MS in the vicinity of T_c [Phys. Rev. B**102**, 014446 (2020)]. In this material, the orbital angular momentum L of Cr originates from the hybridization between Cr and Nb, and L is strongly coupled with the crystal structure [Phys. Rev. B**99**, 174439 (2019)]. The present study clarified that the symmetry of the CrS_6 octahedron is sensitive to H even at room temperature. The paramagnetic spin-orbit coupling should induce the distortion of CrS_6 octahedron, resulting in the changes in Cr-Nb($4f$) distance via the change in the hybridization between Cr-a_{1g} and Nb-$4d_{z^2}$ orbitals.

PACS numbers:

I. INTRODUCTION

In systems with strong magneto-structural correlation, the volume of the unit cell changes when the spin system transforms to a certain magnetically ordered state. This phenomenon is termed as "magnetostriction (MS) effect", and many experimental reports have been published in the fields involving ferromagnetic crystals, alloys, and amorphous alloys [1]. Furthermore, the studies on MS have been enlarged to the first-order transition systems [2], itinerant-electron magnets [3–5], multiferroic systems (perovskite system) including Mn oxides [6–14], heavy fermion systems [15, 16], pyrochlore system [17], and lanthanide-iron compounds [18]. Most of MS effect is related to magnetic ordering, and some of MS is related to crystal fields [19, 20]. In general, the MS in ferromagnets is phenomenologically interpreted as an effect of magnetoelastic coupling, and it is enhanced with the aid of itinerant electrons. From a macroscopic viewpoint, the aforementioned phenomena can be understood with the point group theory.

The MS in the paramagnetic region is rare: It has been observed in several systems such as ferromagnetic amorphous alloys, spin liquid [17], and mixed valence manganese oxides [6, 8], and it is related to the local moments in the paramagnetic state.

The orbital angular momentum L denotes the exotic physical phenomena via the spin-orbit coupling (SOC) that forms a microscopic manner of magneto-structural correlation. The SOC also brings about magnetocrystalline anisotropy, which in turn can enhance the MS effects. In materials, which belongs to Sohncke space group, without rotoinversion symmetry elements [21], the Dzyaloshinskii-Moriya (DM) interaction arises from a combined second-order perturbation of SOC and exchange interaction [22, 23]. The competition between exchange interaction and DM interaction stabilizes a long-wavelength helical order, i.e. helimagnetic (HM) order. The magnitude of DM interaction is generally small when compared to the exchange interaction. However, its vector-type of interaction is rooted in the crystal structure, and governs twisting of spins over the crystal. It brings about nontrivial spin textures such as magnetic superlattice with vortices [24] and kinks [25] at finite magnetic field (H) as well as HM structure at zero H.

The MS effect has been observed in chiral magnets, where the DM interaction can be permitted: For instance, chiral magnets with a B20-type cubic crystal structure allow the existence of multiple DM vectors, and the formation of magnetic vortices lattice called Skyrmion lattice. The H-induced MS, termed forced M-S, related to Skyrmion lattice has been studied in MnSi, via capacitance measurement [26, 27]. The relation of MS to the structural symmetry was discussed based on the group theory [27]. In $Fe_xCo_{i-x}S$ with the B20 type structure, the MS at zero H, termed spontaneous MS,

*Electronic address: mitoh@mns.kyutech.ac.jp

has been investigated from the viewpoint of thermal expansion [28].

In 2020, in a typical monoaxial-DM type of chiral helimagnet $CrNb_3S_6$ with the magnetic ordering temperature T_c of approximately 130 K [29–31], the characteristic spontaneous MS was observed at the boundary between the paramagnetic and helimagnetic states [32]: The change in atomic position, reflecting the existence of local distortion, occurs over a wide temperature range up to room temperature. Note $CrNb_3S_6$ exhibits a strong magnetocrystalline anisotropy on the *ab*-plane [33]. Thus, the forced MS effect was also observed at the strength of a magnetic field H of 1.2 kOe: A small change in the unit cell volume of 0.4% survives even at room temperature [32].

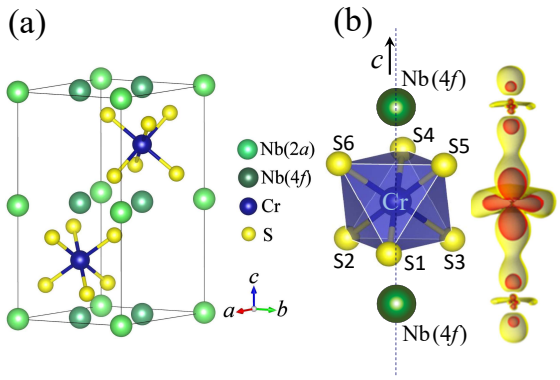

FIG. 1: (Color online) (a) Crystal structure of $CrNb_3S_6$. Nb(2*a*) and Nb(4*f*) are denoted in light and dark green, respectively. (b) Local structure of CrS_6 octahedron sandwiched with two Nb(4*f*) atoms and image of hybridization between Cr-a_{1g} and Nb-$4d_{z^2}$ orbitals. The following relations hold up; ∠S1CrS4 = ∠S2CrS5, ∠S3CrS6. ∠S5CrS6 = ∠S1CrS2, ∠S1CrS3, ∠S2CrS3, ∠S4CrS5, ∠S4CrS6. The two triangles △S1S2S3 and △S4S5S6, are regular triangles.

The crystal structure of $CrNb_3S_6$ is as follows: Cr^{3+} ions are inserted into the space between hexagonal NbS_2 layers as shown in Fig. 1(a). The insertion of Cr^{3+} does break the inversion symmetry. The material crystallizes as the noncentrosymmetric hexagonal space group $P6_322$ [29, 30, 34–36]. The Nb positions occupy two sites, 2*a* and 4*f*, which are termed as Nb(2*a*) and Nb(4*f*) in Fig. 1(a). The Nb(4*f*) is located so as to get close to the 3S triangle of CrS_6 octahedra as shown in Fig. 1(b). However, in this cluster unit of CrS_6-Nb(4*f*), the local symmetry with respect to Cr is approximately D_{3d}. Consequently, Cr 3*d* orbitals leads to an energy splitting of an electron configuration as $t_{2g} \rightarrow e'_g + a_{1g}$. In this case, a_{1g} denotes an orbital, $3z^2-r^2$ that stretches along the *c*-axis toward Nb(4*f*) atoms. The z^2 orbital of Nb(4*f*) is hybridized with the delocalized a_{1g} orbital of Cr [37]. The delocalized e'_g orbital of Cr is hybridized with S 3*p* orbitals.

Based on the Lorenz microscopy experiment, a ferromagnetic network develops on the *ab*-plane [38], and the magnitude of its intraplane interaction is 140 K [33]. The ESR experiment evaluated the interplane exchange interaction along the chiral *c*-axis (16.2 K), the DM interaction (1.29 K), and the easy-plane anisotropy (1.02 K) [39]. The results show fair matching with the values obtained from the Monte Calro simulation [33]. Thus, the ferromagnetic layer (*ab*-plane) with the easy-plane anisotropy stacks along the chiral axis (*c*-axis). The magnetization originates mainly from Cr, while the electrical conductivity originates from Nb. For $T < T_c$, prominent magnetoresistance reflecting the change in the magnetic structure was observed [40–42]. We stress that there is a significant cross correlation among chiral structure, chiral magnetic texture, and electric conductivity, because of the orbital hybridization between Cr and Nb(4*f*). Indeed, the symmetry of CrS_6 octahedron is reduced as the temperature increases above T_c [32]. We are interested in the influence of the symmetry change on the aforementioned cross correlation at room temperature. In this study, to elucidate whether the paramagnetic MS occurs in the microscopic level, we conducted the x-ray structural analysis experiments for $CrNb_3S_6$ as a function of magnetic field H at room temperature.

II. METHODS

Powders and single crystals of $CrNb_3S_6$ were synthesized via a chemical vapor transport method, described elsewhere [38]. The powder sample has also been used in the room-temperature x-ray diffraction (XRD) experiment at hydrostatic pressure [30, 43] and low-temperature XRD at $H = 0$ [32]. In this study, we performed XRD analyses at room temperature (RT), 299.2 K, using a synchrotron radiation XRD system with a cylindrical imaging plate at the Photon Factory at the Institute of Materials Structure Science, High Energy Accelerator Research Organization [44]. The energy of the incident x-rays was 16 keV. Two facing NdFeB magnets (NeoMag Co., Ltd.), product No. N48H with remanence of 13.8 kG and size of 10×6×3 mm^3 and product No. N52 with remanence of 14.5 kG and the size of 10×7×8 mm^3, were located in the aforementioned diffractometer [32]. The H values were changed by controlling the distance between the sample and NdFeB magnets. Then, the H value was always reduced down to zero before constructing new configuration of NdFeB magnets. The experiments for a single crystal of $CrNb_3S_6$ were conducted in three orientations, $H \perp c$ ($H//ab$-plane), 45° orientation from *c*-axis and *ab*-plane, and $H//c$. The accuracy of the orientation adjustment was ±2°. The diffraction spots for single crystals were observed in the vibration mode of every 1° for ±3°. On the basis of the changes in the spot pattern, the changes in the lattice constants were evaluated. Herein, the atomic positions in the unit cell did not become parameters in the analyses. The pattern of observed diffraction spots depend on the H orientation, such that the error bars depend on both the kind of lattice constant (i.e., a or c) and the H orientation.

In the powder experiments, a series of measurements revealed that the quality of the Debye-Scherrer ring did not change even under H. This in turn suggests the crystallite did not orientate along a specific direction under H. The powder diffraction patterns were analyzed to search how each atomic position changes along with the change in lattice constants by means of the Rietveld refinement using the RIETAN-FP package [45].

The H dependence of magnetization (M) was observed using a commercial superconducting quantum interference device magnetometer to confirm the M values and the magnetic irreversibility between field-cooling and field-warming processes. The c-axis of the single crystal was placed in the direction parallel to H or perpendicular to $\vec{H}$. In addition, the electrical resistance R was also observed for $H \perp c$ via the four-terminal method by using a commercial cryostat with a superconducting magnet.

III. EXPERIMENTAL RESULTS

A. Magnetization using a single crystal

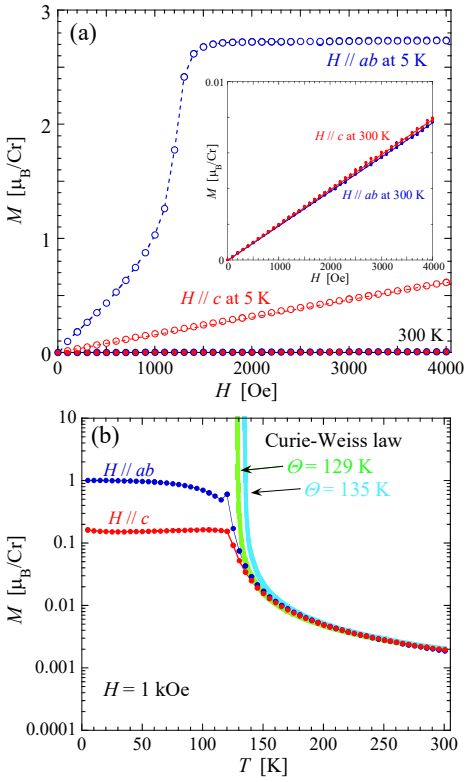

FIG. 2: (Color online) (a) H dependence of magnetization M for $H//c$ and $H \perp c$ at $T = 5$ and 300 K. The results at 300 K are magnified in the inset. (b) T dependence of M for $H//c$ and $H \perp c$ at $H = 1$ kOe. For reference, the curve representing the Curie-Weiss law with the spin value of 3/2 and Weiss temperature (Θ) of 129-135 K is also shown. It indicates that there survives ferromagnetic magnetic correlation between spins of $CrNb_3S_6$ even at 300 K, whereas there is no observable orientation dependence.

Figure 2(a) shows the H dependence of M for $H//c$ and $H \perp c$ at $T = 5$ and 300 K in the H region below 4 kOe. For $H \perp c$ ($H//ab$), M saturates at approximately 3 μ_B at 5 K. For $H//c$, M exhibits a linear increase with respect to the increase in H. However, at 300 K, the values of M are not dependent on the H direction, as confirmed in Fig. 2(b). The T dependence of M in the paramagnetic region obeys the Curie-Weiss law with the spin value of 3/2 and positive Weiss temperature Θ of 129-135 K, consistently with the analytic result in Ref. [29]. Even at around 300 K, the Curie law without the Weiss temperature is inappropriate to reproduce the T dependence. Thus, for $CrNb_3S_6$, thermal fluctuation of 300 K is not sufficient to eliminate the ferromagnetic magnetic correlation between Cr^{3+} spins on the ab-plane.

B. Magnetoresistance using a single crystal

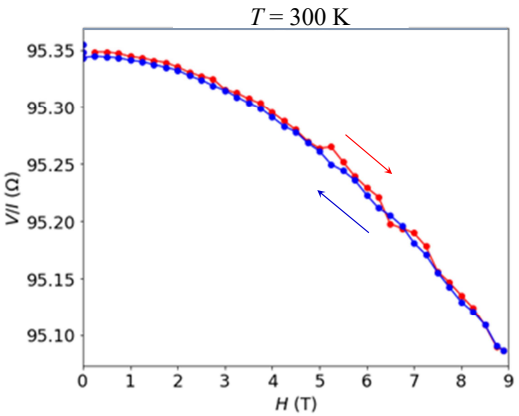

FIG. 3: (Color online) H dependence of electrical resistance R for $H \perp c$ at 300 K in the processes of increasing H (red) and decreasing H (blue). No hysteresis was observed in the magneto resistance response.

Figure 3 shows the H dependence of electrical resistance R at 300 K for $H \perp c$. In the H region up to 9 T, a 0.2% reduction in R was observed. The spontaneous magnetostriction at $H = 0$ and field-forced magnetostriction at $H = 1.2$ kOe have already been observed over 93-295 K [32]. The magnetoresistance was investigated over 10-160 K [41]. In the present study, we confirmed that the significant effect of the hybridization between the z^2 orbital of Nb($4f$) and delocalized a_{1g} orbital of Cr survives even at 300 K. Given the results of Fig. 2(b), it is important to consider that there the Cr^{3+} spins feeling ferromagnetic correlation trigger the magneto-resistance effect by the conduction electrons of Nb.

C. XRD using a single crystal at RT

In $CrNb_3S_6$, the ferromagnetic layer (ab-plane) with the easy-plane anisotropy stacks along the chiral axis (c-

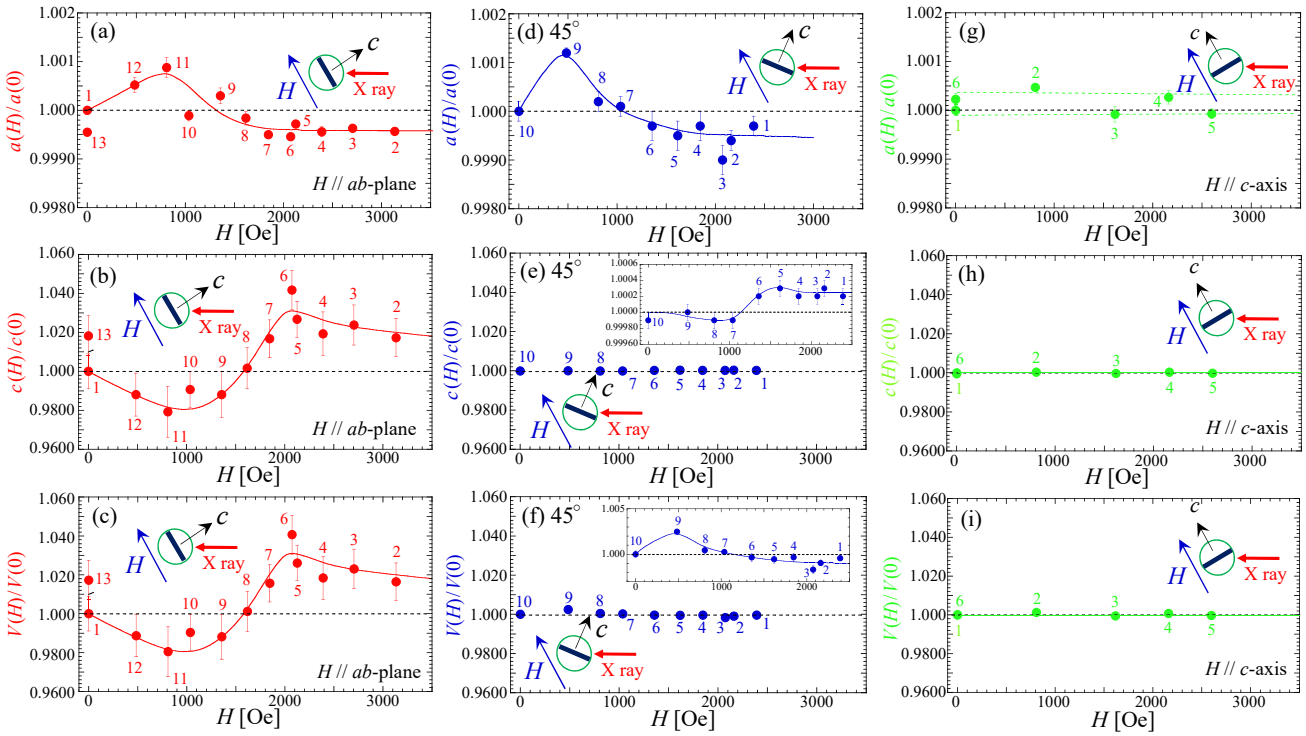

FIG. 4: (Color online) H dependence of lattice constants, a (a, d, g), c (b, e, h), and V (c, f, i), of $CrNb_3S_6$ at RT for $H \perp c$ ($H//ab$-plane) (a-c), the 45° orientation with respect to c-axis and ab-plane (d-f), and $H//c$ (g-i). The numbers adjacent to the symbols denote the sequence of the measurement. The H value was always reduced down to zero before constructing new configuration of NdFeB magnets, and the numbers denoting the sequence have no important meaning in a series of the H change.

axis). The comparison between the magnetostriction for $H//ab$-plane ($H \perp c$) and that for $H//c$ in the single crystal experiments is a matter of the greatest concern.

Figures 4(a, b) show the H dependence of normalized lattice constants a and c with those at $H = 0$ for $H \perp c$ at RT. The lattice expands toward the a-axis at small fields, and the expansion becomes 0.09% at 0.8 kOe. At the same time, c-axis shrinks, which in turn decreases the unit cell volume V as shown in (c). With further increasing H, a starts to decrease. It becomes smaller than that at $H = 0$, and the shrinkage reaches 0.04%. Conversely, c tends to increase around 1 kOe, and it exhibits the 4% expansion at 2 kOe. The 2% expansion remains even above 2.4 kOe, because the value of $c(H)/c(0)$ keeps almost 1.020. The magnitude of the aforementioned forced magnetostriction is much larger than that of the spontaneous magnetostriction below T_c [32]. Thus, the relative change in c is fifty-times larger than that in a. Later, the powder experiment shown below yields microscopic information on a correlation of the structural change in the ab-plane with that along stacking direction of the ab-plane. Now, we assume that the structural change along the c-axis originates from the change in c along the hybridization between z^2 orbital of Nb($4f$) and delocalized a_{1g} orbital of Cr. The change in the unit cell volume V is closely correlated with the change in c. Indeed, their baselines in both c and V exhibit negative slope with respect to H in the considered H region. Hence, in the following we examine as to whether the aforementioned lattice change occurs in other H orientation.

Figures 4(d-f) show the H dependence of normalized a, c, and V when H is applied along the direction that is 45° with respect to the c-axis and ab-plane. The entire H-dependencies of a and c are similar to those for $H \perp c$ ($H//ab$). First, a exhibits small expansion of more than 0.1% at approximately 500 Oe. The maximum expansion is observed at lower H than that for $H \perp c$. Above 1 kOe, the ab-plane shrinks when compared to that at $H = 0$, similarly to $H \perp c$. Next, along the c-axis, shrinkage and expansion occur similarly to that for $H \perp c$, and the switching occurs at 1.2 kOe, which is lower than that for $H \perp c$. The magnitude of the maximum change in c is at most 0.03%. Quantitatively, the change in a is larger than that in c. The change in V shown in (f) reflects that in a rather than that in c. Thus, by deviating the H direction from the ab-plane, the shrinkage-and-expansion along the c-axis is significantly suppressed to the level of one-hundredth.

Figures 4(g-i) show the H dependence of lattice parameters a, c and V for $H//c$. In the figures, a and c do not exhibit meaningful changes with respect to the change in H. Furthermore, V maintains a constant value.

The comparison among three H-orientations in Fig. 4 reveals that the MS occurs when H is applied in a direction parallel to the magnetic easy-plane. It is natural to identify any important factors for producing the easy-plane type of magnetic anisotropy. The present MS at RT is observed sufficiently higher than T_c. The order

of the easy-plane anisotropy ($\sim$ 1 K) as well as the D-M interaction ($\sim$ 1 K) is much smaller than the thermal energy at RT [39]. Hence, it may be worth considering that the paramagnetic MS originates directly from the change in the orbital angular momentum L as opposed to the paramagnetic MS from SOC via spins.

D. XRD using a powder sample at RT

In the case of the powder XRD experiment, the effects of H for all orientations are merged, whereas it is more easier to obtain the information on atomic positions than in the single crystal experiment. To elucidate the mechanism at the unit cell level, each atomic position was investigated in the powder x-ray analysis experiment. As supplemental data, the results for the powder sample are also shown below.

Figures 5(a, b) show the H dependence of lattice constants a and c estimated by the powder XRD analysis at RT. They exhibit a double-maximum at 1.2–1.3 kOe and 2.1–2.3 kOe. The double-maximum in c shifts toward slightly lower H side than that in a. The location of the maximum in c at 2.1 kOe matches that of the maximum in c of the single crystal for $H//ab$ shown in Fig. 4(b). The maximum in a in the lower H side appears at slightly higher H than the maximum in a of the single crystal for $H//ab$ shown in Fig. 4(a). This behavior is almost consistent with the behavior observed in the experiment for 45° orientation with respect to c-axis and ab-plane using a single crystal (see Fig. 4(d-f))). Comparing the maximum change in $a(H)/a(0)$ [0.023 %] and that in $c(H)/c(0)$ [0.025 % from the baseline], they are comparable, and both changes are reflected in $V(H)/V(0)$.

Figures 5 (d-g) show the H dependence of atomic positions Nb($4f$)z, Sx, Sy, and Sz. Specifically, Nb($4f$)z exhibits the maximum at approximately 800 and 2000 Oe. Sx exhibits the maximum at approximately 1200 and 1800 Oe, Sy exhibits the maximum at approximately 1900 Oe, and Sz exhibit prominent minimum at approximately 1000 Oe and tiny hump at approximately 1800 Oe. These changes should be correlated with the change in lattice parameters a, c, and V. Indeed, we found the following correlation among them: The maximum in a at approximately 1300 Oe and 2250 Oe are related with the change in the lower-side maximum in Sx and the maximum in Sy, respectively. The movement of Nb($4f$) along the z direction (c-aixs direction) would be related with a change in the atomic coordinates of S. In this compound, the orbital hybridization between Cr and Nb($4f$) produces an angular momentum L [37]. Hence, it is evident that the change in Nb($4f$)z leads to a change in L. The change in atomic coordinates is reflected in the change in the bonding angle, S1-Cr-S4, S1-Cr-S5, S1-Cr-S6, and S5-Cr-S6, as shown in Figs. 5(h-k). They show characteristic changes at approximately 1200 and 1800 Oe. Specifically, S1-Cr-S4 tends to change far from 180° at two characteristic fields, and S1-Cr-S5, S1-Cr-S6, and S5-Cr-S6 tend to change far from 90° at two characteristic fields. At approximately 1200 and 1800 Oe, the CrS_6 octahedra tend to be distorted, and there the twisting can be enhanced.

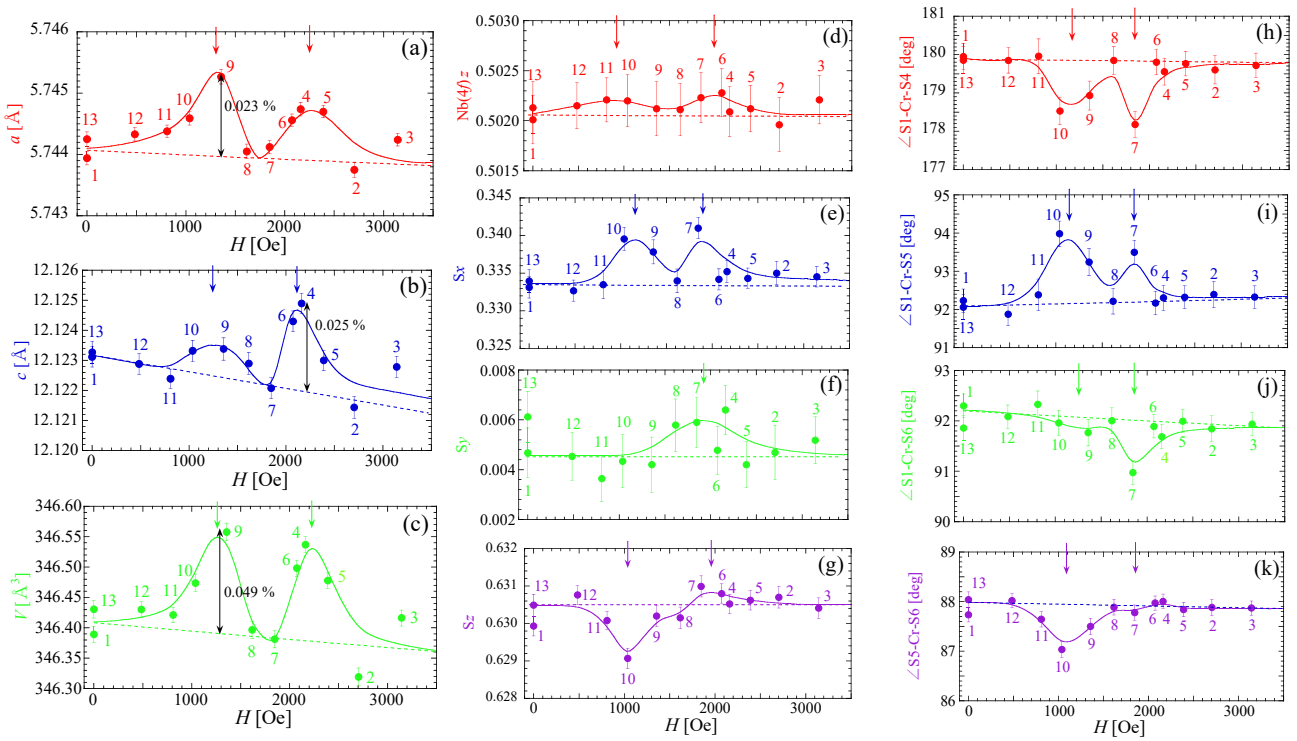

FIG. 5: (Color online) H dependence of lattice constants [a (a), c (b), V (c)], atomic positions [Nb(4f)z (d), Sx (e), Sy (f), Sz (g)], and the bonding angles [S1-Cr-S4 (h), S1-Cr-S5 (i), S1-Cr-S6 (j), S5-Cr-S6 (k)], obtained via powder XRD analysis of $CrNb_3S_6$ at RT. In (a)-(c), for the point with the maximum change, the relative value with respect to the baseline is depicted along with a two-way arrow. The numbers adjacent to the symbols denote the sequence of the measurement. The H value was always reduced down to zero before constructing new configuration of NdFeB magnets, and the numbers denoting the sequence have no important meaning in a series of the H change. In each figure, characteristic H values are marked with arrows.

IV. DISCUSSION

Figure 6 shows the overview of the change in the twisting of twin CrS_3-tetrahedrons in the process of increasing H wherein the H region is divided into four regions by focusing five H points. The aforementioned five H points are denoted with blue circles in the two insets of Fig. 6, which present the H dependence of ∠S1-Cr-S4 (a) and Cr-Nb(4f) (b). Herein, ∠S1-Cr-S4 is one of characteristic angles for imaging the twisting of twin CrS_3-tetrahedrons, and the distance Cr-Nb(4f) is valid for imaging the change in the hybridization between Cr and Nb(4f) along the z direction.

(1): In the process of 0 → 1.0 kOe (No. 1 → No. 10), the area of the 3S triangle, △S1S2S3 and △S4S5S6, decreases, while the distance between the two 3S triangles increases. The upper inverse-pyramid rotates to counterclockwise, while the lower pyramid rotates to clockwise. The aforementioned change reveals that the strain due to the twisting increases in this process.

(2): In the process of 1.0 → 1.6 kOe (No. 10 → No. 8), the area of the 3S triangle increases, while the distance between two 3S triangles decreases. Consequently, the relative inverse-twisting of two pyramids is released, and the strain accumulated in the process of (1) is released.

(3): In the process of 1.6 → 1.8 kOe (No. 8 → No. 7), structural change similar to that in (1) occurs.

(4): In the process of 1.8 → 2.7 kOe (No. 7 → No. 2), structural change similar to that in (2) occurs.

Thus, the accumulation and release of the twisting-induced strain are repeated. In the actual experiment, the measurement sequence was No.1 → 2 → 7 → 8 → 10. Furthermore, the measurement sequence after No. 2 was not performed in the process of decreasing H systematically, nevertheless we can consistently see double maximum or double minimum H dependence in most of figures in Fig. 5. The present H dependence of attractive structural parameters is surely reversible against the increase and decrease in H.

By focusing the CrS_6 octahedra and the hybridization between Cr and Nb(4f), the changes in the unit cell volume under magnetic field are imaged: The heavy Nb(4f) atom moves along the c-axis is related with the rotation of the CrS_6 octahedra. This movement brings about a change in a as well as a change in c. Hence, it is important to consider as to "why the aforementioned structural changes occur?".

As the first scenario, we assume that Cr-a_{1g} orbital can change by SOC via the Cr spins when H is parallel to the

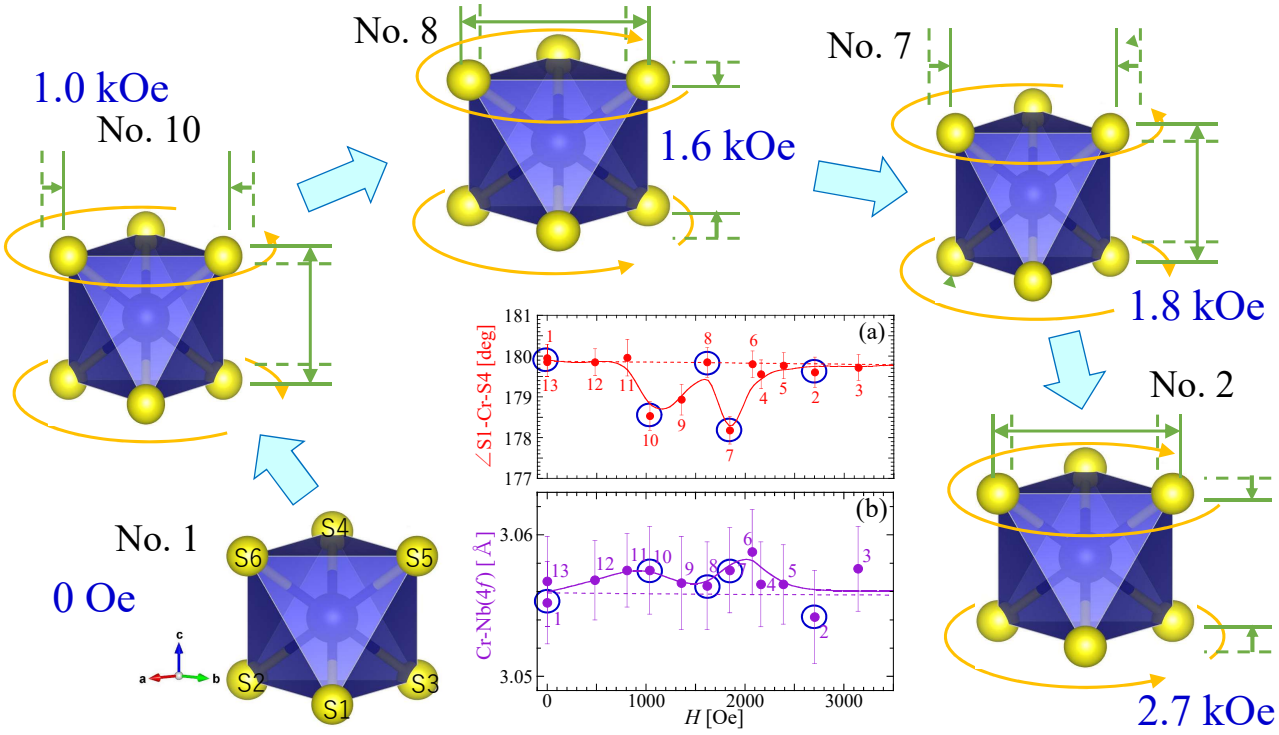

FIG. 6: (Color online) Overview of the change in the twisting of twin CrS_3-pyramids in the process of increasing H, whrere the H region is divided into four regions. The number for each structural image corresponds to the sequence number of the experiment using the powder sample. For reference, it is marked with a blue circle in two inset figures, (a) ∠S1-Cr-S4(H) (it is the same to Fig. 5(h)) that is one of characteristic angles for imaging the twisting of twin CrS_3-tetrahedrons, and (b) distance Cr-Nb($4f$) valid for imaging the change in the hybridization between Cr and Nb($4f$) along the z direction (c-axis direction). The green broken lines denote the situation before the change, and the solid green lines denote the situation after the change. The orange arrows denote the direction of twisting. In the actual experiment, the measurement sequence was No.1 → 2 → 7 → 8 → 10.

ab-plane. This leads to the change in a accompanying the distortion of the CrS_6 octahedron. This change in a leads to the change in c through the hybridization between Cr-a_{1g} and Nb-$4d_{z^2}$ orbitals. As the second scenario, H directly changes the orbital angular momentum L for Cr, leading to a change in the hybridization between Cr-a_{1g} and Nb-$4d_{z^2}$ orbitals. Consequently, the change in the hybridization brings about the change in the unit cell volume.

The characteristic H values for the structural change at RT are observed as identical to the critical H values between CSL-1 and CSL-2 and between CSL-2 and FFM [31]. Theoretically, the former is related to J and D, while the latter is related to J. However, occasional consistency cannot be explained: The magnetic moment at RT is one-thousandth of that below T_c. However, SOC governs the magneto-structural correlation even above T_c (=127 K) [32]: Even at $H = 0$, the Invar effect, which maintains the constant unit cell volume, is observed below 170 K [32]. With respect to the coordinate of Nb($4f$) and S, significant changes are observed over the wide T range up to RT. In particular, Nb($4f$)z has the minimum at around 260 K and Sz exhibits large change above T_c. The symmetry of the CrS_6 octahedron is reduced as T increases above T_c [32]. In the present study, the magneto-structural correlation at RT was investigated via the examination of MS. The paramagnetic moment with ferromagnetic magnetic correlation exits even at RT, as seen in Fig. 2(b). The ferromagnetic correlation works on the ab-plane, and indeed the MS effects is observed remarkably for $H//ab$-plane. Herein, the MS cannot be discussed without considering the spin as well as orbital. Therefore, we propose the first scenario, the paramagnetic MS is triggered with SOC. In future, the first-principles calculations would be desired to understand the paramagnetic magnetostriction at room temperature.

V. CONCLUSION

In this study, we observed magnetostriction in $CrNb_3S_6$ at room temperature. This intrinsically differs from forced magnetostriction due to the SOC in the vicinity of T_c. The distortion of the CrS_6 octahedron accompanies a change in the hybridization between Cr-

a_{1g} and Nb-$4d_{z^2}$ orbitals, resulting in the change in the Cr-Nb($4f$) distance. The resultant movement of Nb($4f$) along the z direction leads to a change in the unit cell volume. This is a unique phenomenon of the L-induced structural modulation or small-S-motivated SOC.

The crystal structure can be modified via L. Now, it is an open question as to whether the present paramagnetic MS is triggered from the change in L directly changed by H, or from the change in S and the subsequent change in SOC. In this material, the total magnetization at room temperature is quite small due to large thermal fluctuation, whereas the ferromagnetic spin contribution cannot be ignored there. We consider that the present paramagnetic magnetostriction would originate from significant SOC in $CrNb_3S_6$.

Acknowledgments

This study was supported by Grants-in-Aid for Scientific Research, Grant No. (S) 25220803, from the Ministry of Education, Culture, Sports, Science and Technology (MEXT), Japan. This study was also supported by the Centre for Chiral Science at Hiroshima University (the MEXT program for promoting the enhancement of research universities, Japan) and JSPS Core-to-Core Program, A. Advanced Research Networks.

[1] A. Goldman, *Handbook of Modern Ferromagnetic Materials* (Springer Science & Business Media, 1999).
[2] K. Irisawa, A. Fujita, and K. Fukamichi, J. Appl. Phys. **93**, 7266 (2003).
[3] S. Khmelevskyi and P. Mohn, Phys. Rev. B **69**, 140404(R) (2004).
[4] P. Gegenwart, F. Weickert, R. Perry, and Y. Maeno, Physica B **378** (2006).
[5] T. Sakon, Y. Yamasaki, H. Kodama, T. Kanomata, H. Nojiri, and Y. Adachi, Materials **12**, 3655 (2019).
[6] J. M. D. Teresa, M. R. Ibarra, J. Blasco, J. García, C. Marquina, P. A. Algarabel, Z. Arnold, K. Kamenev, C. Ritter, and R. von Helmolt, Phys. Rev. B **54**, 1187 (1996).
[7] C. Ramos, H. Salva, R. Sanchez, M. Tovar, F. Rivadulla, J. Mira, J. Rivas, A. Lopez-Quintela, L. Hueso, M. Saint-Paul, et al., J. Magn. Magn. Mater. **226** (2001).
[8] C. Marquina, M. Ibarra, A. Abramovich, A. Michurin, and L. Koroleva, J. Magn. Magn. Mater. **226** (2001).
[9] A. Abramovich, R. Demin, L. Koroleva, A. Michurin, O. Gorbenko, A. Kaul, R. Szymczak, and B. Krzymanska, Planet. Space Sci. **189**, 907911 (2002).
[10] R. Mahendiran, M. R. Ibarra, C. Marquina, B. Garcia-Landa, L. Morellon, A. Maignan, B. Raveau, A. Arulraj, and C. N. R. Rao, Appl. Phys. Lett. **82**, 242 (2003).
[11] Y. Yamato, M. Matsukawa, T. Kumagai, R. Suryanarayanan, S. Nimori, M. Apostu, A. Revcolevschi, K. Koyama, and N. Kobayashi, Phys. Rev. B **78**, 132411 (2008).
[12] L. I. Koroleva, D. M. Zashchirinskiĭ, T. M. Khapaeva, L. I. Gurskiĭ, N. A. Kalanda, V. M. Trukhan, R. Szymczak, and B. Krzumanska, Sov. Phys. Solid State **52**, 96 (2010).
[13] Y. S. Oh, B.-G. Jeon, S. Y. Haam, S. Park, V. F. Correa, A. H. Lacerda, S.-W. Cheong, G. S. Jeon, and K. H. Kim, Phys. Rev. B **83**, 060405(R) (2011).
[14] Y. Ma, J. Cong, and Y. Sun, J. Phys.: Condens. Matter **31**, 205701 (2019).
[15] P. Morin, J. Rouchy, and G. Creuzet, J. Magn. Magn. Mater. **69**, 99 (1987).
[16] J. Yoshida, S. Abe, D. Takahashi, Y. Segawa, Y. Komai, H. Tsujii, K. Matsumoto, H. Suzuki, and Y. Ōnuki, Phys. Rev. Lett. **101**, 256402 (2008).
[17] J. P. C. Ruff, Z. Islam, J. P. Clancy, K. A. Ross, H. Nojiri, Y. H. M. andH. A. Dabkowska, A. D. Dabkowski, and B. D. Gaulin, Phys. Rev. Lett. **105**, 077203 (2011).
[18] M. A. El-Aal, L. Kazokova, V. Chechernicov, and A. Chermushkina, J. Magn. Magn. Mater. **74**, 248 (1998).
[19] T. Takeuchi, P. Ahmet, M. Abliz, R. Settai, and Y. Ōnuki, J. Phys. Soc. Jpn. **65**, 1404 (1996).
[20] V. M. T. S. Barthem, D. Gignoux, A. Nacht-Saada, D. Schmitt, and G. Creuzet, Phys. Rev. B **37**, 1733 (1988).
[21] U. Müller., *Symmetry Relationships between Crystal Structures. Applications of Crystallographic Group Theory in Crystal Chemistry.* (Oxford University Press, Oxford, 2013).
[22] I. E. Dzyaloshinskii, J. Phys. Chem. Solid **4**, 241 (1958).
[23] T. Moriya, Phys. Rev. **120**, 91 (1960).
[24] A. Bogdanov and A. Hubert, J. Magn. Magn. Mater. **138**, 255 (1994).
[25] Y. Togawa, Y. Kousaka, K. Inoue, and J. Kishine, J. Phys. Soc. Jpn. **85**, 112001 (2016).
[26] M. Matsunaga, Y. Ishikawa, and T. Nakajima, J. Phys. Soc. Jpn. **51**, 1153 (1982).
[27] S. Wang, Y. Hu, J. Tang, W. Wei, J. Cong, Y. Sun, H. Du, and M. Tian, New J. Phys. **21**, 123052 (2019).
[28] K. Shimizu, H. Maruyama, H. Yamazaki, and H. Watanabe, J. Phys. Soc. Jpn. **59**, 305 (1990).
[29] T. Miyadai, K. Kikuchi, H. Kondo, S. Sakka, M. Arai, and Y. Ishikawa, J. Phys. Soc. Jpn. **52**, 1394 (1983).
[30] M. Mito, T. Tajiri, K. Tsuruta, H. Deguchi, J. Kishine, K. Inoue, Y. Kousaka, Y. Nakao, and J. Akimitsu, J. Appl. Phys. **117**, 183904 (2015).
[31] K. Tsuruta, M. Mito, H. Deguchi, J. Kishine, Y. Kousaka, J. Akimitsu, and K. Inoue, Phys. Rev. B **93**, 104402 (2016).
[32] T. Tajiri, M. Mito, Y. Kousaka, J. Akimitsu, J. Kishine, and K. Inoue, Phys. Rev. B **102**, 014446 (2020).
[33] M. Shinozaki, S. Hoshino, Y. Masaki, J. Kishine, and Y. Kato, J. Phys. Soc. Jpn. **85**, 074710 (2016).
[34] A. R. Beal, *in Intercalated Layered Materials,* edited by F. A. Levy (D. Reidel Publishing Company, Dordecht, Holland, 1979).
[35] F. Hulliger and E. V. A. Pobitschka, J. Solid State Chem. **1**, 117 (1970).
[36] L. M. Volkova and D. V. Marinin, J. Appl. Phys. **116**,

133901 (2014).
[37] M. Mito, H. Ohsumi, T. Shishidou, F. Kuroda, M. Weinert, K. Tsuruta, Y. Kotani, T. Nakamura, Y. Togawa, J. Kishine, et al., Phys. Rev. B **99**, 174439 (2019).
[38] Y. Togawa, T. Koyama, K. Takayanagi, S. Mori, Y. Kousaka, J. Akimitsu, S. Nishihara, K. Inoue, A. S. Ovchinnikov, and J. Kishine, Phys. Rev. Lett. **108**, 107202 (2012).
[39] D. Yoshizawa, J. Kishine, Y. Kousaka, Y. Togawa, M. Mito, J. Akimitsu, K. Inoue, and M. Hagiwara, Phys. Proc. **75**, 926 (2015).
[40] Y. Togawa, Y. Kousaka, S. Nishihara, K. Inoue, J. Akimitsu, A. S. Ovchinnikov, and J. Kishine, Phys. Rev. Lett. **111**, 197204 (2013).
[41] Y. Togawa, T. Koyama, Y. Nishimori, Y. Matsumoto, S. McVitie, D. McGrouther, R. L. Stamps, Y. Kousaka, J. Akimitsu, S. Nishihara, et al., Phys. Rev. B **92**, 220412 (2015).
[42] L. Wang, N. Chepiga, D.-K. Ki, L. Li, F. Li, W. Zhu, Y. Kato, O. S. Ovchinnikova, F. Mila, I. Martin, et al., Phys. Rev. Lett. **118**, 257203 (2017).
[43] M. Mito, S. Tominaga, Y. Komorida, H. Deguchi, S. Takagi, Y. Nakao, Y. Kousaka, and J. Akimitsu, J. Phys: Conference Series **215**, 012182 (2010).
[44] A. Fujiwara, K. Ishii, T. Watanuki, H. Suematsu, H. Nakao, K. Ohwada, Y. Fujii, Y. Murakami, T. Mori, H. Kawada, et al., J. Appl. Cryst. **33**, 1241 (2000).
[45] F. Izumi and K. Momma, Solid State Phenom. **130**, 15 (2007).